

# Widespread global increase in intense lake phytoplankton blooms since the 1980s

<https://doi.org/10.1038/s41586-019-1648-7>

Jeff C. Ho<sup>1,2\*</sup>, Anna M. Michalak<sup>1\*</sup> & Nima Pahlevan<sup>3,4</sup>

Received: 11 January 2018

Accepted: 6 August 2019

Published online: 14 October 2019

Freshwater blooms of phytoplankton affect public health and ecosystem services globally<sup>1,2</sup>. Harmful effects of such blooms occur when the intensity of a bloom is too high, or when toxin-producing phytoplankton species are present. Freshwater blooms result in economic losses of more than US\$4 billion annually in the United States alone, primarily from harm to aquatic food production, recreation and tourism, and drinking-water supplies<sup>3</sup>. Studies that document bloom conditions in lakes have either focused only on individual or regional subsets of lakes<sup>4–6</sup>, or have been limited by a lack of long-term observations<sup>7–9</sup>. Here we use three decades of high-resolution Landsat 5 satellite imagery to investigate long-term trends in intense summertime near-surface phytoplankton blooms for 71 large lakes globally. We find that peak summertime bloom intensity has increased in most (68 per cent) of the lakes studied, revealing a global exacerbation of bloom conditions. Lakes that have experienced a significant ( $P < 0.1$ ) decrease in bloom intensity are rare (8 per cent). The reason behind the increase in phytoplankton bloom intensity remains unclear, however, as temporal trends do not track consistently with temperature, precipitation, fertilizer-use trends or other previously hypothesized drivers. We do find, however, that lakes with a decrease in bloom intensity warmed less compared to other lakes, suggesting that lake warming may already be counteracting management efforts to ameliorate eutrophication<sup>10,11</sup>. Our findings support calls for water quality management efforts to better account for the interactions between climate change and local hydrological conditions<sup>12,13</sup>.

The reported incidence of toxic phytoplankton blooms has risen considerably over the past half-century<sup>14</sup>. While it is generally understood that nutrient loading drives phytoplankton blooms<sup>15</sup>, the degree to which bloom conditions are changing globally and the factors that drive these changes among multiple interacting stressors<sup>16</sup> are still uncertain<sup>17</sup>. An understanding of global patterns, trends and drivers is necessary, however, for designing effective management and remediation strategies<sup>18</sup>. Whereas past studies synthesizing information on the long-term trends in phytoplankton blooms of lakes have been limited by data availability, recent advances in cloud-based parallel computing have made it possible to leverage high-resolution freely accessible satellite imagery over large areas, enabling the study of long-term environmental trends on a global scale<sup>19,20</sup>.

Here, we take advantage of these advances to generate a long-term record of intense, near-surface phytoplankton blooms for dozens of large lakes across the globe. We use data from the Landsat 5 satellite to generate time series of peak summer bloom intensity from 1984 to 2012 for 71 lakes in 33 countries across 6 continents (Fig. 1). In total, the data span 30,922 scenes and 72.6 billion lake pixels. The study lakes span a broad range of physical characteristics and degree of anthropogenic impacts (Supplementary Table 1; see Methods for a full description of the implemented approach). Seasonal peak bloom intensity for a given

lake and year is defined based on the maximum observed lake-wide near-infrared signal magnitude, with a first-order correction of atmospheric interference using the shortwave-infrared signal<sup>21</sup>. Remotely sensed observations within the near-infrared part of the electromagnetic spectrum are sensitive to intense, near-surface algal blooms (see Methods). An initial superset of 154 lakes was selected based on their inclusion in previous studies that leveraged remote sensing by satellites<sup>22,23</sup>, thus reducing the likelihood that persistent cloudiness obscured the images. These lakes all have surface areas of more than 100 km<sup>2</sup>; globally, lakes within this size range contain approximately 95% of all water stored in lakes<sup>24</sup>. Data of lakes for which little signal was observed throughout the study period, as well as data of lakes for which the signal was far outside the range over which the original algorithm was designed<sup>21</sup>, were removed. A smaller number of additional lakes were removed due to previously documented evidence of a lack of phytoplankton blooms. Of the final selected lakes, 38 have a documented presence of harmful cyanobacterial species, while the rest show evidence of other phytoplankton species (10 lakes) or no reported evidence of blooms (23 lakes). Given the heterogeneity in lake characteristics, the time series of the interannual bloom intensity for each lake is normalized by its own long-term mean and s.d. to assess the relative change in bloom intensity over time. This approach eliminates the need to compare absolute

<sup>1</sup>Department of Global Ecology, Carnegie Institution for Science, Stanford, CA, USA. <sup>2</sup>Department of Civil and Environmental Engineering, Stanford University, Stanford, CA, USA. <sup>3</sup>NASA Goddard Space Flight Center, Greenbelt, MD, USA. <sup>4</sup>Science Systems and Applications Inc, Lanham, MD, USA. \*e-mail: jeffho@stanford.edu; michalak@stanford.edu

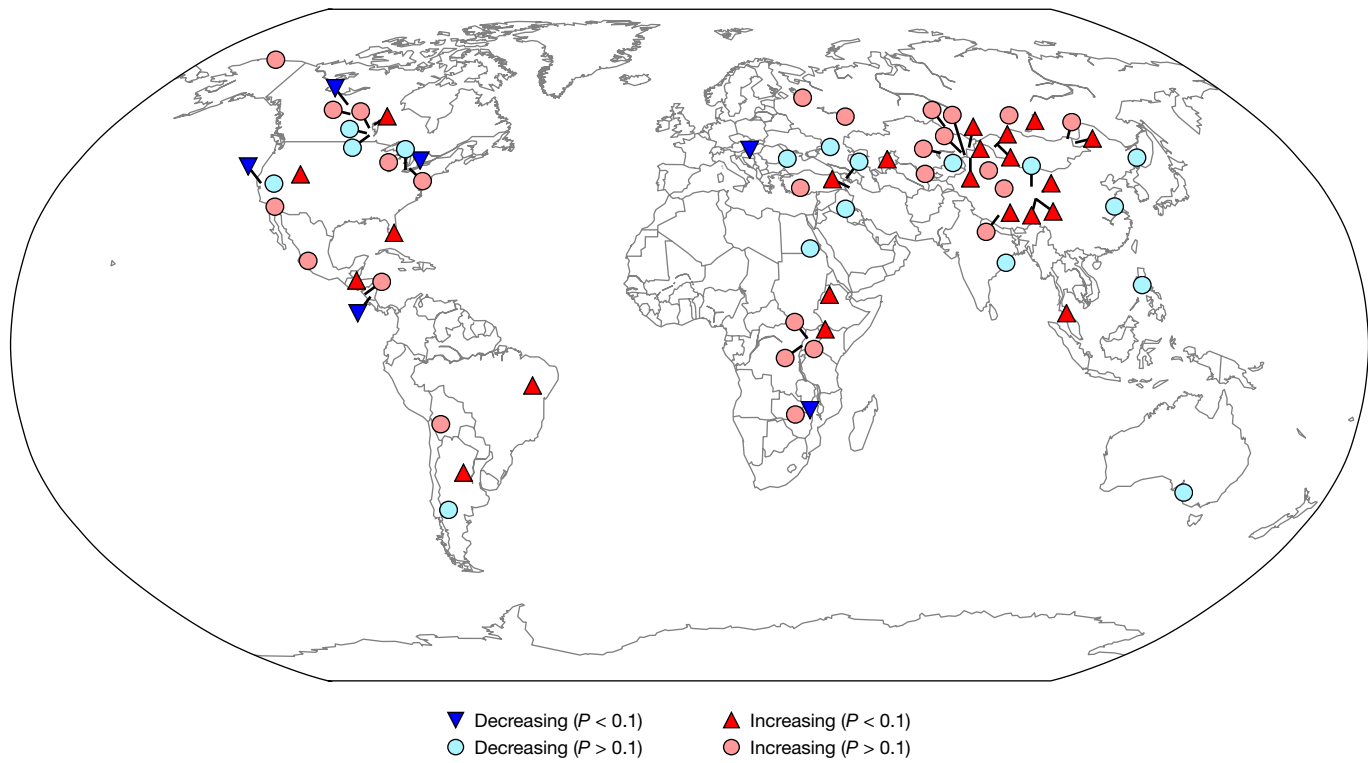


**Fig. 1 | Global distribution of lake bloom intensity trends shows that the peak summertime bloom intensity has increased since the 1980s.** The map shows bloom intensity trends for all 71 study lakes for the period 1984–2012 (Supplementary Table 1). Colours and symbols indicate whether the bloom

intensity decreased (blue) or increased (red), and whether the trend is statistically significant (triangles for  $P < 0.1$ ; circles for  $P > 0.1$ ). The base map was generated using Generic Mapping Tools<sup>33</sup>.

magnitudes across lakes, which has been an important barrier to past syntheses across lakes<sup>25</sup>.

We find that the implemented algorithm is able to successfully capture previously documented spatial gradients in the severity of phytoplankton blooms within individual lakes and temporal trends in phytoplankton bloom intensity for specific lakes (Extended Data Fig. 1 and Methods). Using simulations of atmospheric radiative transfer, we also find that the algorithm is insensitive to reported variations in Landsat 5 orbit or image radiometric quality, primarily owing to the strong signal that arises from the intense, near-surface blooms identified in study lakes (see Supplementary Information). These results suggest that a single algorithm can indeed identify intense phytoplankton blooms despite the large differences in optical properties across lakes<sup>26</sup>, as long as the focus is on interannual rather than inter-lake variability. This lends support to the approach implemented in this study for tracking long-term trends globally. We then used all 71 study lakes to assess global trends in summertime peak phytoplankton bloom intensity. We also used a subset of 49 lakes with at least 14 years of data to explore more detailed historical temporal patterns in phytoplankton bloom conditions, for which the 14-year threshold was selected on the basis of previously published studies on global lake temperatures<sup>22,27</sup>.

We find that peak summertime phytoplankton bloom intensity has increased in more than two-thirds of study lakes since the 1980s (48 out of 71 lakes) (Fig. 1). Increases in bloom intensity are statistically significant for close to a third of all lakes ( $P < 0.1$  for 22 out of 71 lakes), whereas only 6 lakes exhibited a statistically significant decrease in intensity ( $P < 0.1$ ). A similar proportion of lakes has an increasing bloom intensity among those with a documented presence of cyanobacteria (24 out of 38 lakes) compared to lakes without cyanobacteria (24 out of 33 lakes), and the proportion of lakes with increases in bloom intensity is also consistent across lakes with different areas, volumes, mean and maximum depths, and latitudes (see Supplementary Table 1 and Supplementary

Information). These results suggest that the observed trends are widespread globally and across lake types, in contrast to previous hypotheses of differential impacts as a function of latitude<sup>28</sup> or morphometry<sup>29</sup>. This finding provides a global perspective that is consistent with surveys of sedimentary records across temperate–subarctic lakes<sup>6</sup> that show sharp increases in the concentrations of cyanobacterial pigments after 1985. This finding also corroborates putative trends of increasing harmful cyanobacterial blooms globally<sup>17</sup>, and counters the hypothesis that increased reporting of toxic blooms is instead a by-product of increased scientific attention<sup>30</sup>.

We find that lake phytoplankton bloom histories follow one of four prototypical pathways, termed here ‘sustained improvement’, ‘improvement then deterioration’, ‘deterioration’ and ‘no significant trend’ (Fig. 2a–d and Methods). The two pathways that include deteriorating conditions reveal that increases in peak bloom intensity occurred predominantly in the latter half of the study period (Fig. 2b, c). For example, three-quarters of study lakes (51 out of 68) with sufficient data for the second half of the study period (1998–2012) exhibited an increase in bloom intensity during this period, whereas only a third (22 out of 66) experienced an increase during the first half (1984–1997). The reason behind the temporal coherence of changes in phytoplankton bloom intensity remains unclear, as temporal trends do not track consistently with temperature, precipitation, fertilizer-use trends, satellite data availability or geomorphological characteristics of individual lakes (Extended Data Figs. 2–5 and Supplementary Information), nor are there widespread trends in the seasonal timing of peak bloom intensity (see Supplementary Information).

We find that although lakes that exhibited sustained improvement were rare ( $n = 6$ ), they experienced less warming (or more cooling) relative to those that exhibited improvement then deterioration ( $P = 0.09$ ; Fig. 3 and Extended Data Fig. 6), suggesting that lake warming may have counteracted management efforts in the latter group. This finding suggests that nutrient reduction targets based on historical relationships

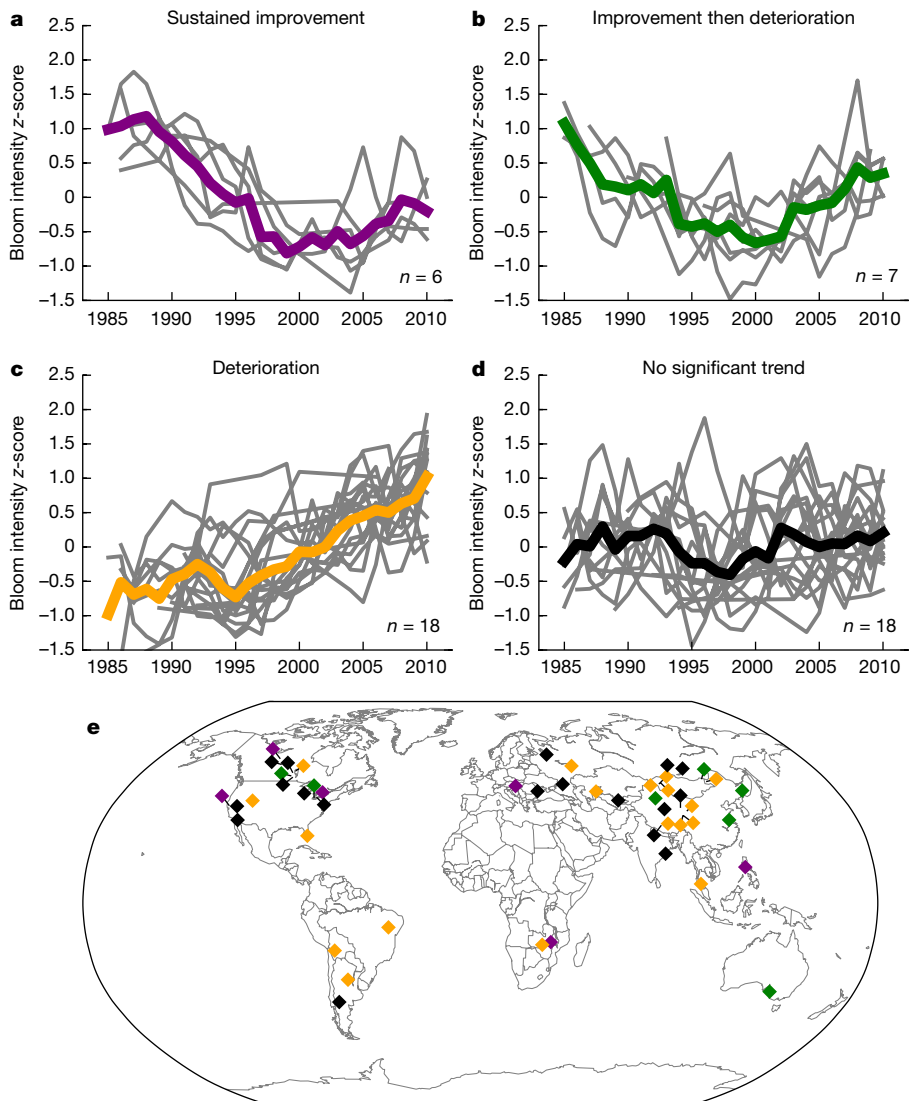


**Fig. 2 | Lake bloom histories follow one of four prototypical pathways.**

**a–d**, Time series for lakes with at least 14 years of data ( $n = 49$ ) categorized by historical pathway. Grey lines show 5-year moving averages of normalized bloom intensity, with coloured lines showing pathway averages across lakes. The time

series of the bloom intensity z-score for each lake is calculated using its own historical mean and s.d. **e**, Global distribution of lake pathways. The base map was generated using Generic Mapping Tools<sup>33</sup>.

between bloom severity and nutrient loading may have to be revised in the context of climate change, as has been hypothesized<sup>11</sup>. Generalizing the impact of warming across a wide range of lakes is inadvisable, however, as trends across the full lake ensemble showed little direct

correlation with temperature (Fig. 4, Extended Data Figs. 2, 3 and Supplementary Information). Rather, these findings suggest that the effects of global lake warming differ depending on lake-specific characteristics<sup>31</sup>, and highlight the importance of assessing the role of lake attributes in modulating the impact of temperature on nutrient–phytoplankton relationships<sup>32</sup>.

Overall, this study provides a global view of trends in intense lacustrine near-surface phytoplankton blooms over the past three decades. We examine bloom histories for lakes with widely differing characteristics and geographical locations, and demonstrate the promise of long-term satellite observations for tracking intense bloom conditions across a heterogeneous set of systems to augment geographically and temporally limited in situ monitoring efforts. Our results corroborate the putative reported increase in bloom occurrence and intensity globally, and highlight that lakes that have exhibited a long-term decrease in bloom intensity are rare. Results further show that sustained decreases in bloom intensity are more likely to have occurred in lakes with little or no warming, suggesting that rising lake temperatures may hamper environmental recovery, and illustrating the importance of identifying factors that make some lakes more susceptible to the effects of warming.

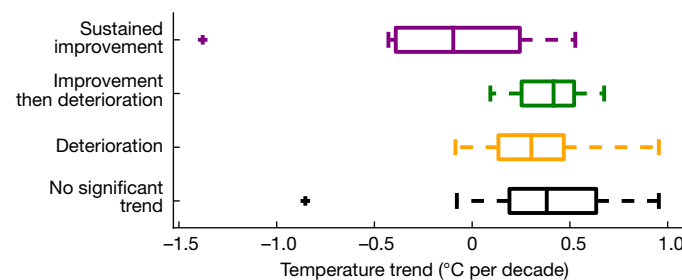
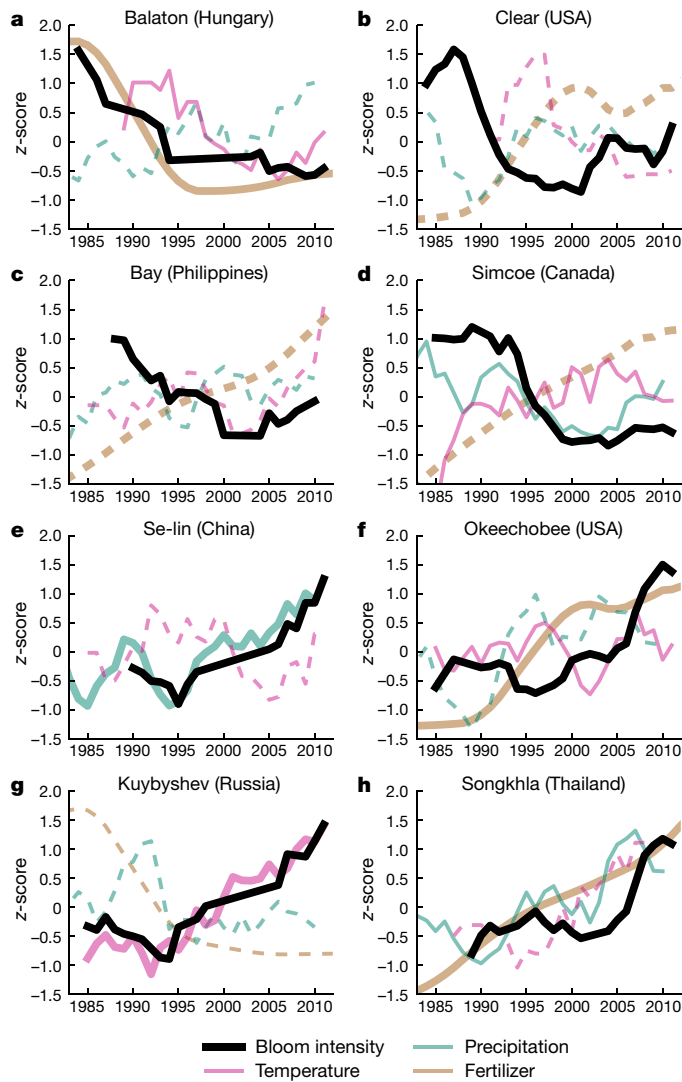


**Fig. 3 | Lakes that experienced improvements in bloom conditions tend to have experienced little to no warming.** Box plots of the water temperature trend (1985–2012) binned by lake historical pathway. Each box extends from the first to the third quartile values, with a line at the median. The whiskers extend to  $1.5 \times$  the interquartile range from the edges of the box. The plus symbols show outlier values past the end of the whiskers.



1. Pick, F. R. Blooming algae: a Canadian perspective on the rise of toxic cyanobacteria. *Can. J. Fish. Aquat. Sci.* **73**, 1149–1158 (2016).
2. Ndlela, L. L., Oberholster, P. J., Van Wyk, J. H. & Cheng, P. H. An overview of cyanobacterial bloom occurrences and research in Africa over the last decade. *Harmful Algae* **60**, 11–26 (2016).
3. Kudela, R. M. et al. *Harmful Algal Blooms. A Scientific Summary For Policy Makers* (IOC/UNESCO, 2015).
4. Hampton, S. E. et al. Sixty years of environmental change in the world's largest freshwater lake – Lake Baikal, Siberia. *Glob. Change Biol.* **14**, 1947–1958 (2008).
5. Duan, H. et al. Two-decade reconstruction of algal blooms in China's Lake Taihu. *Environ. Sci. Technol.* **43**, 3522–3528 (2009).
6. Tararu, Z. E. et al. Acceleration of cyanobacterial dominance in north temperate–subarctic lakes during the Anthropocene. *Ecol. Lett.* **18**, 375–384 (2015).
7. Carvalho, L. et al. Sustaining recreational quality of European lakes: minimizing the health risks from algal blooms through phosphorus control. *J. Appl. Ecol.* **50**, 315–323 (2013).
8. Beaulieu, M., Pick, F. & Gregory-Eaves, I. Nutrients and water temperature are significant predictors of cyanobacterial biomass in a 1147 lakes data set. *Limnol. Oceanogr.* **58**, 1736–1746 (2013).
9. Kosten, S. et al. Warmer climates boost cyanobacterial dominance in shallow lakes. *Glob. Change Biol.* **18**, 118–126 (2012).
10. Posch, T., Köster, O., Salcher, M. M. & Pernthaler, J. Harmful filamentous cyanobacteria favoured by reduced water turnover with lake warming. *Nat. Clim. Change* **2**, 809–813 (2012).
11. Paerl, H. W. et al. Mitigating cyanobacterial harmful algal blooms in aquatic ecosystems impacted by climate change and anthropogenic nutrients. *Harmful Algae* **54**, 213–222 (2016).
12. Winder, M. Lake warming mimics fertilization. *Nat. Clim. Change* **2**, 771–772 (2012).
13. Paerl, H. W. & Huisman, J. Blooms like it hot. *Science* **320**, 57–58 (2008).
14. Carmichael, W. in *Cyanobacterial Harmful Algal Blooms: State of the Science and Research Needs* (ed. Hudnell, H. K.) 105–125 (Springer-Verlag, 2008).
15. Schindler, D. W., Carpenter, S. R., Chapra, S. C., Hecky, R. E. & Orihel, D. M. Reducing phosphorus to curb lake eutrophication is a success. *Environ. Sci. Technol.* **50**, 8923–8929 (2016).
16. Winter, J. G., Young, J. D., Landre, A., Stainsby, E. & Jarjanazi, H. Changes in phytoplankton community composition of Lake Simcoe from 1980 to 2007 and relationships with multiple stressors. *J. Great Lakes Res.* **37**, 63–71 (2011).
17. Huisman, J. et al. Cyanobacterial blooms. *Nat. Rev. Microbiol.* **16**, 471–483 (2018).
18. McCrackin, M. L., Jones, H. P., Jones, P. C. & Moreno-Mateos, D. Recovery of lakes and coastal marine ecosystems from eutrophication: a global meta-analysis. *Limnol. Oceanogr.* **62**, 507–517 (2017).
19. Gorelick, N. et al. Google Earth Engine: planetary-scale geospatial analysis for everyone. *Remote Sens. Environ.* **202**, 18–27 (2017).
20. Zhu, Z. et al. Benefits of the free and open Landsat data policy. *Remote Sens. Environ.* **224**, 382–385 (2019).
21. Ho, J. C., Stumpf, R. P., Bridgeman, T. B. & Michalak, A. M. Using Landsat to extend the historical record of lacustrine phytoplankton blooms: a Lake Erie case study. *Remote Sens. Environ.* **191**, 273–285 (2017).
22. Schneider, P. & Hook, S. J. Space observations of inland water bodies show rapid surface warming since 1985. *Geophys. Res. Lett.* **37**, L22405 (2010).
23. Sharma, S. et al. A global database of lake surface temperatures collected by in situ and satellite methods from 1985–2009. *Sci. Data* **2**, 150008 (2015).
24. Messager, M. L., Lehner, B., Grill, G., Nedeva, I. & Schmitt, O. Estimating the volume and age of water stored in global lakes using a geo-statistical approach. *Nat. Commun.* **7**, 13603 (2016).
25. Hampton, S. E. Understanding lakes near and far. *Science* **342**, 815–816 (2013).
26. Spyralos, E. et al. Optical types of inland and coastal waters. *Limnol. Oceanogr.* **63**, 846–870 (2018).
27. O'Reilly, C. M. et al. Rapid and highly variable warming of lake surface waters around the globe. *Geophys. Res. Lett.* **42**, 10,773–10,781 (2015).
28. Downing, J. in *Global Environmental Change* (ed. Freedman, B.) 221–229 (Springer, 2014).
29. Kraemer, B. M. et al. Morphometry and average temperature affect lake stratification responses to climate change. *Geophys. Res. Lett.* **42**, 4,981–4,988 (2015).
30. Fristach, A. et al. in *Cyanobacterial Harmful Algal Blooms: State of the Science and Research Needs* (ed. Hudnell, H. K.) 45–103 (Springer-Verlag, 2008).
31. Adrian, R. et al. Lakes as sentinels of climate change. *Limnol. Oceanogr.* **54**, 2,283–2,297 (2009).
32. Rigosi, A., Carey, C. C., Ibelings, B. W. & Brookes, J. D. The interaction between climate warming and eutrophication to promote cyanobacteria is dependent on trophic state and varies among taxa. *Limnol. Oceanogr.* **59**, 99–114 (2014).
33. Wessel, P., Smith, W. H. F., Scharroo, R., Luis, J. & Wobbe, F. Generic Mapping Tools: improved version released. *Eos* **94**, 409–410 (2013).

**Publisher's note** Springer Nature remains neutral with regard to jurisdictional claims in published maps and institutional affiliations.

© The Author(s), under exclusive licence to Springer Nature Limited 2019

## METHODS

### Satellite source data and implementation of the bloom detection algorithm

We used all Landsat 5 Thematic Mapper (L5 TM) images over study lakes (1984–2012) that covered the five months encompassing summer (June to October or December to April, depending on lake latitude, similar to a global study of satellite-estimated lake temperatures<sup>22</sup>). Given its long-term archive, L5 TM can be used to assess bloom severity in the upper layer of the water column<sup>21,34</sup>. Our analysis used images from the L5 TM top-of-atmosphere (TOA) reflectance image collection in Google Earth Engine<sup>35</sup>, collected originally from the US Geological Survey<sup>36</sup>. The images in this collection represent unitless planetary TOA reflectance ( $\rho_\lambda$ )<sup>37</sup>:

$$\rho_\lambda = \frac{\pi L_\lambda d^2}{\text{ESUN}_\lambda \cos(\theta_s)} \quad (1)$$

where  $L_\lambda$  is the spectral radiance at the sensor's aperture ( $\text{W}(\text{m}^2 \text{sr} \mu\text{m})^{-1}$ ),  $d$  is the Earth–Sun distance (astronomical units),  $\text{ESUN}_\lambda$  is the mean exoatmospheric solar irradiance ( $\text{W}(\text{m}^2 \mu\text{m})^{-1}$ ) and  $\theta_s$  is the solar zenith angle (degrees). L5 TM Surface Reflectance products<sup>38</sup> were not available worldwide for the full period at the time of algorithm development<sup>21</sup>.

We implemented a compositing technique to create images covering the whole surface area of each lake. On the basis of the 16-day revisit period of Landsat, we created composites for each lake by stitching together all L5 TM scenes overlapping with the lake during 16-day time intervals. For each year, intervals started on the first day of the first month analysed (either 1 June or 1 December) and ran until 144 days later, or 9 intervals total. Overlapping pixels from multiple scenes were averaged in each final composite. Artefacts of this process were observed for some lakes (for example, horizontal or vertical stripes at scene boundaries), but were not found to substantially affect subsequent analyses.

To mask land within each 16-day composite image, we modified lake polygons from the Global Lakes and Wetlands Database<sup>39</sup>. The original polygons were adjusted manually to fully cover the lake surface area based on images with maximum lake extent over the study period. Within these polygons, we used the Fmask algorithm<sup>40,41</sup>, as implemented in Google Earth Engine<sup>42</sup>, to exclude cloud and cloud shadow pixels, and to identify the water surface area in each composite. We tested the use of other cloud detection algorithms (for example, the Landsat Automatic Cloud Cover Assessment procedure<sup>43</sup>), but Fmask resulted in fewer misclassification errors due to turbid water and haze. We also tested static land cover maps to mask land pixels, but the Fmask water layer better accounted for dynamic changes in lake shorelines over time.

We then applied a bloom detection algorithm based on the near-infrared band, using the shortwave-infrared (SWIR) band to minimize effects of atmospheric interference and a 'greenness' filter to distinguish suspended sediment<sup>21</sup>. The algorithm subtracts the pixel value in the SWIR band (L5 TM band 5, 1.55–1.75  $\mu\text{m}$ ), weighted with an empirical parameter, from the value in the near-infrared band (L5 TM band 4, 0.76–0.90  $\mu\text{m}$ ) as a measure of near-surface bloom intensity:

$$B = F_G(\rho_{B4} - 1.03\rho_{B5}) \quad (2)$$

where  $B$  is the bloom intensity, ranging from 0 to 0.1 where 0.1 generally represents intense near-surface phytoplankton blooms,  $\rho_{B4}$  is L5 TM TOA band 4,  $\rho_{B5}$  is L5 TM TOA band 5 and  $F_G$  represents the greenness filter that masks out pixels below a certain hue ( $H$ ) threshold based on L5 TM TOA in bands 1, 2, and 3:

$$F_G = \begin{cases} 1 & \text{if } H < 1.6 \\ 0 & \text{if } H > 1.6 \end{cases} \quad (3)$$

$$H = \begin{cases} \frac{\rho_{B2} - \rho_{B1}}{\rho_{B3} + \rho_{B2} - 2\rho_{B1}} & \text{if } \rho_{B1} = \min(\rho_{B1}, \rho_{B2}, \rho_{B3}) \\ \frac{\rho_{B3} - \rho_{B2}}{\rho_{B3} + \rho_{B1} - 2\rho_{B2}} + 2 & \text{if } \rho_{B2} = \min(\rho_{B1}, \rho_{B2}, \rho_{B3}) \\ \frac{\rho_{B1} - \rho_{B3}}{\rho_{B2} + \rho_{B1} - 2\rho_{B3}} + 1 & \text{if } \rho_{B3} = \min(\rho_{B1}, \rho_{B2}, \rho_{B3}) \end{cases} \quad (4)$$

Under intense, near-surface algal bloom conditions, backscattering due to phytoplankton abundance dominates the water-leaving radiance in the near-infrared range that is otherwise damped by pure water absorption<sup>44,45</sup> (Extended Data Figs. 7, 8; see Supplementary Information for additional discussion of algorithm sensitivity to in situ bloom conditions). Although this approach has proven effective in identifying the extent of near-surface intense phytoplankton blooms, we emphasize that the retrieval of concentrations of specific bloom severity metrics (for example, chlorophyll- $a$ ) is beyond the scope of this study.

### Selection of the initial 76 study lakes

We first selected 154 lakes from those included in a study of global lake temperatures<sup>23</sup> with temperature data collected by satellite. The rationale for choosing these lakes was twofold: (1) there was a lower likelihood of persistent cloudiness obscuring images because these lakes had previously been successfully explored using satellite remote sensing and (2) the in situ temperature data for other lakes were not collected in a consistent way that would be representative of the whole lake (for example, some data points were collected at point locations on specific shores of the lake).

After an initial exploration of three randomly selected years of composite images for each lake, we sub-selected 95 lakes for analysis based on the criteria that lake pixels have non-zero bloom intensity values below a threshold of 0.1 in a substantial portion of images. We did this to identify lakes that had ranges of bloom intensity values most similar to Lake Erie, for which the algorithm was originally validated<sup>21</sup>. Compared to the 59 lakes that were not selected, these 95 lakes in general were shallower and had smaller lake volume, suggesting that the approach may have been more applicable for detecting blooms in shallower lakes.

We then performed a literature search to explore whether the observed bloom intensity signal in lakes was likely to be indicative of real phytoplankton blooms (of any type) or a false-positive result. We used ISI Web of Science, Google Scholar and Google Search for the lake name, lake name + "algal bloom" and lake name + "eutrophic". Based on the results of this search, we determined that 78 lakes had either some evidence of phytoplankton blooms (51 out of 78) or no evidence against phytoplankton blooms (27 out of 78), whereas the remaining 17 lakes had strong evidence against the signal representing phytoplankton blooms (for example, in one lake a high bloom intensity signal was erroneously caused by high ice reflectance). Two lakes were also removed from the dataset at this stage based on a lack of L5 TM data during the study period (that is, data were available for only one or two years).

The remaining 76 lakes were selected for further analysis. In these lakes, 54% had support from the literature for evidence of presence of cyanobacteria, with 29% of lakes specifically dominated by *Microcystis* sp. In total, 10,892 composites were compiled from 30,922 L5 TM scenes during the selected months across study lakes, with a median of 139 composites and 283 scenes per lake. The total number of composites per lake ranged from 24 for Lake Edward (43 scenes total) to 250 for Lake Winnipeg (1,771 scenes total). Lakes with a greater number of scenes tended to be in North America, as expected based on historical L5 TM coverage<sup>46</sup>. The number of years with available data per lake ranged from 5 to 28 years with a mean of 21 years (Supplementary Table 1); among lakes with at least 14 years of data, the mean was 22 years per lake.

## Validation of well known spatial gradients in bloom intensity

We further evaluated the proposed approach by comparing geographical regions within lakes with known spatial gradients of bloom intensity. We searched the literature for descriptions of spatial gradients for the 76 study lakes, for example, on the basis of chlorophyll-*a* or phytoplankton biomass observations, and then examined algorithm output values in regions that would be expected to show the largest differences. Using this approach, we identified 48 pairs of regions across 22 lakes (Supplementary Table 2). For instance, in Lake Balaton we identified three regions based on documented chlorophyll-*a* and biomass gradients from the southwest to the northeast<sup>47–49</sup>. The southwest basins are eutrophic to hypertrophic, the northeast basin is mesotrophic and the middle basin is in-between<sup>47</sup>; the expectation is therefore that bloom intensities would be higher in a region in the southwest basin relative to a region in the middle basin, which would then also be higher relative to a region in the northeast basin.

We documented the expected bloom intensity in each region qualitatively (that is, high, medium or low) as well as the strength of the evidence supporting the expected direction of the gradient between regions (that is, strong, medium or weak) (for example, some are based on extensive in situ sampling over many years, whereas others are based on more qualitative inferences). For each of the 48 pairs of regions, we computed the difference in intensity between regions by comparing the mean intensity across all pixels within each region of the lake over the full study period.

The gradient between regions that was inferred using the implemented algorithm was in the correct direction for over three-quarters of region pairs (37 out of 48 pairs). For the Lake Balaton example described earlier, all three comparisons between mean pixel values in the three regions were consistent with the expected sign of the difference in bloom intensity (high versus medium, high versus low, medium versus low).

The previously published evidence was not strong for 10 out of the 11 pairs of regions for which the gradient was in the direction opposite to the expected direction. For example, two pairs were for Songkhla Lake, where the evidence on the spatial gradient came from one publication that was not peer-reviewed and another that was based purely on computational modelling rather than in situ observations<sup>50,51</sup>. Because the vast majority of the discrepancies in identifying spatial gradients were for region pairs with weaker support in the literature, results indicate that the implemented algorithm is able to identify well established spatial gradients in bloom intensity across a variety of lakes.

We note that the qualitative approach used here represents a first step towards understanding how global patterns in bloom intensity may be measured using satellite remote sensing. Although the algorithm used here was validated quantitatively for data from only Lake Erie, the results of our qualitative approach together with atmospheric radiative transfer simulations (see Supplementary Information), indicate that the algorithm provides a useful signal of bloom intensity for the lakes analysed in this study. Additional validation may be needed for other applications.

## Generation of bloom intensity time series and trends

To generate long-term time series of summertime maximum bloom intensities for each lake, we summed the algorithm output values over the whole lake for each composite, as a measure of bloom intensity. This approach assumes that the algorithm output value is correlated with measures such as near-surface chlorophyll-*a* or phytoplankton biomass, which is supported by validation based on well known spatial gradients, as described above. We took the largest composite bloom intensity each year as an estimate of summertime maximum bloom intensity, similar to other studies<sup>21,52</sup>. This approach focuses on the relative spatial intensity of phytoplankton blooms over time, and therefore minimizes the impact of noise in L5 TM images over bodies of water<sup>53</sup>.

We removed estimates from each time series when the observed lake surface area was less than 80% of maximum, or less than the mean minus one s.d. of the whole surface area of the lake for the time series, whichever was lower. These guidelines were determined heuristically, based on removing composites that visually had large portions of the lake surface area unavailable due either to missing L5 TM scenes or high cloud cover. We also removed estimates for years in which there were fewer than 3 composites due to missing data, as these were expected to be less representative of the summertime maximum. Main findings were not found to be sensitive to minor variations in these thresholds.

We further adjusted for variations in observed lake surface due to clouds or missing L5 TM scenes by dividing the annual bloom intensity estimates by the observed surface area of each lake in each year. This had the benefit of correctly adjusting observed bloom severity trends for lakes where the water surface area changed substantially over time. For example, for a subset of lakes that have dried up during the study period (for example, Lake Urmia or the Aral Sea), a decline in water surface area would otherwise be incorrectly observed as a decline in bloom intensity. Normalizing by water surface area more accurately reflects the true bloom conditions in those lakes over time. Although, in principle, this could also make blooms of constant severity in an otherwise shrinking lake appear to have an increasing trend, this scenario was not found among study lakes with declining water surface area. Given the highly varying local conditions for study lakes with respect to bloom intensity and water surface area trends with time, normalizing by water surface area provided the best approach overall for accounting for variations due to clouds and missing L5 TM scenes.

Finally, to compare data across different lakes, we normalized the annual time series of the peak bloom intensity for each lake by its own long-term mean and s.d. values, creating bloom intensity z-scores. This is similar to other studies that have treated historical bloom data from remote sensing<sup>54</sup>, tracked long-term trends in cyanobacteria<sup>6</sup> or estimated long-term trends of other parameters in lakes<sup>27</sup>.

## Evaluation of bloom intensity time series and trends

To further evaluate the implemented approach, we compared the temporal evolution of peak bloom intensity in well studied lakes to those described in existing literature, and also compared bloom intensity trends overall to trends in the SWIR TOA reflectance.

From each time series of normalized annual peak bloom intensity, we tested for the presence of monotonic time trends using the *S* statistic from the Mann–Kendall trend test<sup>55</sup> and estimated the magnitude of temporal trends using Thiel–Sen’s slope<sup>56</sup>. These tests are both non-parametric procedures that are known to be more robust to outliers and more accurate for skewed or heteroskedastic data<sup>57</sup> and have been used widely for assessing temporal trends in limnologic studies and those evaluating trends in phytoplankton blooms specifically<sup>6,31,58,59</sup>. Trend analyses over the whole study period were performed for all lakes ( $n = 76$ ).

For lakes in which large changes in bloom intensity have been documented for the study period, the data used here accurately matched both the direction and timing of changes described in the literature. For example, substantial improvements in bloom conditions have been reported for Lake Balaton<sup>60,61</sup>, Clear Lake<sup>62,63</sup> and Lake Simcoe<sup>16,64</sup>, and all showed statistically significant ( $P < 0.1$ ) decreases in peak bloom intensity in the data presented here over the same timeframes as described in previous studies. The improvement in water quality of Lake Balaton that occurred in the 1990s, which coincided with sewage controls and a decline in agriculture<sup>61</sup>, was reproduced correctly in the time series (Fig. 4a). Clear Lake experienced a similar decline in bloom intensity in the 1990s—probably due to the trophic cascade stemming from drought<sup>63</sup>—that was also correctly reproduced (Fig. 4b). Furthermore, for Lake Simcoe, an improvement in water quality that occurred soon after 1995, which coincided with a widespread invasion of zebra

mussels<sup>16,65,66</sup>, was also successfully reproduced (Fig. 4d). The developed data similarly reproduced histories for lakes with documented increases in bloom intensity during the study period, such as Lake Winnipeg<sup>67</sup> and Lake Baikal<sup>14,88</sup>, and captured documented temporal patterns of decreasing and increasing bloom intensities in ecosystems as diverse as Lake Erie<sup>68</sup> and Tsimlyansk Reservoir<sup>69</sup> (Extended Data Fig. 9).

We further evaluated the performance of the approach for the detection of false-positive (that is, high derived bloom intensity for low bloom intensity spectra) and false-negative (that is, low derived bloom intensity for high bloom intensity spectra) results using the atmospheric radiative transfer simulations described in the Supplementary Information. The analyses demonstrated the robustness of the algorithm in limiting false-positive results—that is, correctly identifying instances in which no blooms were present. However, the analyses also identified that aerosol optical thickness (AOT) has an effect on the incidence of false-negative results whereby a higher AOT (for example, hazy conditions) resulted in an increased likelihood that high bloom intensity events were missing.

Because SWIR can be used as a proxy for AOT, we next evaluated whether derived bloom intensity trends in study lakes could erroneously be due to trends in aerosol conditions that affect the likelihood of false-negative results. This was accomplished by comparing peak bloom intensity trends to trends in the SWIR TOA reflectance. For five lakes with statistically significant trends ( $P < 0.1$ ) in both peak bloom intensity and SWIR TOA reflectance, we found that observed bloom intensity trends coincided with trends in SWIR TOA reflectance, increasing the risk that apparent trends in bloom intensity could be due to a change in the likelihood of false-negative results. For these lakes, peak bloom intensity and SWIR trends were in opposite directions (that is, increasing SWIR resulting in an increased likelihood of false-negative results consistent with a decreased bloom intensity trend, and vice versa for decreasing SWIR). Decreasing bloom intensity trends were observed in four of the five lakes (Chao, Gaoyou, Taihu and Sarykamshskoye), with an increasing bloom intensity trend observed in the fifth (Kremenshugskoye). Increasing SWIR trends in the four lakes were consistent with trends in aerosols in Eastern China and central Asia over the study period<sup>70</sup>, whereas a reduction in aerosols in Eastern Europe<sup>70</sup> was consistent with the latter. Because we could not confirm whether or not the observed bloom intensity trends were in fact attributable to trends in SWIR, to be conservative we removed these five lakes from the subsequent analysis. This resulted in a final set of  $n = 71$  lakes for further analysis. For trends estimated over shorter periods (1984–1997 and 1998–2012), slightly fewer lakes were used ( $n = 66$  and  $n = 68$ , respectively) because at least two years of observations per period were required to compute trends. A subset of lakes with at least 14 years of data ( $n = 49$ ) was also used to explore temporal patterns in peak bloom intensity.

Beyond this analysis of SWIR trends, we found no other evidence that any potential misclassification of bloom intensity trends occurred. To assess whether our approach could have been incorrectly measuring trends in other environmental variables, we explored historical patterns of potential confounders that have been documented in the literature. Trends in Secchi depth did not match the observed bloom intensity trends (for example, in Lake Simcoe<sup>71</sup>, Great Salt Lake<sup>72</sup> or Lake Okeechobee<sup>73</sup>), indicating a lack of evidence to suggest that the implemented algorithm was potentially measuring other constituents of water quality. Nor did we find any evidence that global changes in atmospheric constituents, such as aerosols, dust and water vapour, could explain the overall geographical pattern of bloom observations (except in the five aforementioned lakes), because such constituents have a spatial coherence at large regional scales<sup>70,74–76</sup> whereas the observed lake trends were highly spatially heterogeneous (Fig. 1). For individual lakes, bloom intensity trends also did not track well with observed trends in submerged aquatic vegetation (for example, Lake Okeechobee<sup>73</sup>), gypsum (for example, Salton Sea<sup>77</sup>) or cloud cover (for example, Lake Nicaragua<sup>78</sup>). Taken together, this suggested that our findings about

the global proportion of lakes with increasing bloom intensity trends were likely to be robust.

### Characteristics of the final 71 study lakes

The 71 study lakes (Supplementary Table 1) spanned a wide range of surface areas (158 to 67,052 km<sup>2</sup>) and maximum depth (2 to 1,637 m) comparable to previous global studies of lakes<sup>29</sup>. Of the 49 lakes with at least 14 years of bloom data, a large majority warmed over the study period (88%) (Extended Data Fig. 6), with the temperature trend ranging from -1.40 °C per decade (that is, cooling) to 0.93 °C per decade. Most of these 49 lakes also experienced an increase in annual precipitation (61%, ranging from -49 to 173 mm per decade) while close to half of the lakes experienced an increase in fertilizer application rate (49%, ranging from -1.47 to 2.41 Mg N km<sup>-2</sup> per decade) (Supplementary Table 1).

### Categorization of lakes by prototypical historical pathway

To bin the lakes by prototypical historical pathway, we fit a linear model with time for each lake time series using ordinary least squares regression:

$$y = \beta_1 t + \beta_0 \quad (5)$$

where  $y$  represents the normalized maximum summertime bloom intensity,  $t$  represents the year of the observation, and  $\beta_1$  and  $\beta_0$  are the fitted model parameters. Bloom intensity values from individual lake pixels ( $B$  from Eq. (2)) were summed for each image composite, and the maximum summed bloom intensity for each year was used to create the time series  $y$  after correcting for missing data, subtracting the long-term mean and dividing by the long-term s.d. Lakes for which the linear term was statistically significant ( $P < 0.1$ ) were categorized as sustained improvement if the peak bloom intensity trend decreased with time ( $\beta_1 < 0$ ) and deterioration if the peak bloom intensity trend increased with time ( $\beta_1 > 0$ ).

For the remaining lakes, we fit a quadratic model to each lake time series:

$$y = \beta_2 t^2 + \beta_1 t + \beta_0 \quad (6)$$

where a third term is added indicating a change in peak bloom intensity with  $t^2$ . Lakes for which the quadratic term was statistically significant ( $P < 0.1$ ) and  $\beta_2 > 0$  were categorized as improvement then deterioration. The remaining lakes were categorized as no significant trend.

This approach used both simple monotonic trends with time as well as an assessment of the degree of improvement and deterioration to categorize bloom intensity trends. Categorization of lakes (eutrophication, restoration or no change) on the basis of simple changes in lake parameters (increasing, decreasing or no consistent change, respectively) has been used previously to understand long-term trends<sup>6</sup>, as have comparisons of multiple measurements over time to assess the balance between historical deterioration and improvement<sup>18</sup>.

### Data availability

The Landsat 5 Thematic Mapper imagery used in this study is available from the US Geological Survey (<http://earthexplorer.usgs.gov>) and through Google Earth Engine (<https://earthengine.google.com>). The bloom intensity trend estimates, historical pathway categories and environmental driver variables generated for each lake and analysed in this study are provided in Supplementary Table 1. The temperature, precipitation, fertilizer use and lake geomorphological data supporting the findings of this study are publicly available<sup>23,79,80</sup> (see ‘Environmental driver, watershed, and geomorphological characteristic data sets’ in the Supplementary Information).

## Code availability

Google Earth Engine's web interface allows the bloom detection algorithm<sup>21</sup> to be applied on any Landsat 5 Thematic Mapper images. Access will be provided upon request.

34. Tebbs, E. J., Remedios, J. J. & Harper, D. M. Remote sensing of chlorophyll-a as a measure of cyanobacterial biomass in Lake Bogoria, a hypertrophic, saline-alkaline, flamingo lake, using Landsat ETM+. *Remote Sens. Environ.* **135**, 92–106 (2013).
35. Google. Earth Engine. <https://earthengine.google.com/> (2016).
36. USGS. Landsat Missions. <http://landsat.usgs.gov/> (2016).
37. Chander, G., Markham, B. L. & Helder, D. L. Summary of current radiometric calibration coefficients for Landsat MSS, TM, ETM+, and EO-1 ALI sensors. *Remote Sens. Environ.* **113**, 893–903 (2009).
38. USGS. Landsat Surface Reflectance Level-2 Data Products. <https://landsat.usgs.gov/landsat-surface-reflectance-data-products> (2017).
39. Lehner, B. & Döll, P. Development and validation of a global database of lakes, reservoirs and wetlands. *J. Hydrol.* **296**, 1–22 (2004).
40. Zhu, Z. & Woodcock, C. E. Object-based cloud and cloud shadow detection in Landsat imagery. *Remote Sens. Environ.* **118**, 83–94 (2012).
41. Zhu, Z., Wang, S. & Woodcock, C. E. Improvement and expansion of the Fmask algorithm: cloud, cloud shadow, and snow detection for Landsats 4–7, 8, and Sentinel 2 images. *Remote Sens. Environ.* **159**, 269–277 (2015).
42. Erickson, T. A. Earth Engine Data Catalog: USGS Landsat 5 TOA Reflectance (Orthorectified) with Fmask. [https://code.earthengine.google.com/dataset/LANDSAT\\_LT5\\_L1T\\_TOA\\_FMASK](https://code.earthengine.google.com/dataset/LANDSAT_LT5_L1T_TOA_FMASK) (2016).
43. Irish, R. R. Landsat 7 automatic cloud cover assessment. In Proc. SPIE 4049, *Algorithms for Multispectral, Hyperspectral, and Ultraspectral Imagery VI* 348–355 (2000).
44. Moore, T. S. et al. Bio-optical properties of cyanobacteria blooms in western Lake Erie. *Front. Mar. Sci.* **4**, 300 (2017).
45. Gower, J., King, S., Borstad, G. & Brown, L. Use of the 709 nm band of MERIS to detect intense plankton blooms and other conditions in coastal waters. *ESA J.* **1161**, 365–368 (2005).
46. Goward, S. et al. Historical record of Landsat global coverage: mission operations, NSLRSDA, and international cooperators stations. *Photogramm. Eng. Remote Sensing* **72**, 1155–1169 (2006).
47. Palmer, S. C. J. et al. Validation of Envisat MERIS algorithms for chlorophyll retrieval in a large, turbid and optically-complex shallow lake. *Remote Sens. Environ.* **157**, 158–169 (2015).
48. Pálffy, K., Présing, M. & Vörös, L. Diversity patterns of trait-based phytoplankton functional groups in two basins of a large, shallow lake (Lake Balaton, Hungary) with different trophic state. *Aquat. Ecol.* **47**, 195–210 (2013).
49. Hajnal, É. & Padisák, J. Analysis of long-term ecological status of Lake Balaton based on the ALMOBAL phytoplankton database. *Hydrobiologia* **599**, 227–237 (2008).
50. Chesooh, S., Lim, A. & Tongkumchum, P. Trend of water quality and model for forecasting eutrophication occurrence in Songkhla Lake, Thailand. in Proc. Taal2007: The 12th World Lake Conference 834–839 (2008).
51. Suwanidcharoen, S. & Liengcharernsir, W. Development of phytoplankton model with application to Songkhla Lake, Thailand. *Lowl. Technol. Int.* **14**, 50–59 (2012).
52. Stumpf, R. P., Wynne, T. T., Baker, D. B. & Fahnenstiel, G. L. Interannual variability of cyanobacterial blooms in Lake Erie. *PLoS ONE* **7**, e42444 (2012).
53. Pahlevan, N., Balasubramanian, S. V., Sarkar, S. & Franz, B. A. Toward long-term aquatic science products from heritage Landsat missions. *Remote Sens.* **10**, 1337 (2018).
54. Palmer, S. C. J. et al. Satellite remote sensing of phytoplankton phenology in Lake Balaton using 10 years of MERIS observations. *Remote Sens. Environ.* **158**, 441–452 (2015).
55. Mann, H. B. Nonparametric tests against trend. *Econometrica* **13**, 245–259 (1945).
56. Sen, P. K. Estimates of the regression coefficient based on Kendall's tau. *J. Am. Stat. Assoc.* **63**, 1379–1389 (1968).
57. Rousseeuw, P. J. & Leroy, A. M. *Robust Regression and Outlier Detection* (John Wiley & Sons, 1987).
58. Izmost'eva, L. R. et al. Lake-wide physical and biological trends associated with warming in Lake Baikal. *J. Great Lakes Res.* **42**, 6–17 (2016).
59. Gobler, C. J. et al. Ocean warming since 1982 has expanded the niche of toxic algal blooms in the North Atlantic and North Pacific oceans. *Proc. Natl Acad. Sci. USA* **114**, 4975–4980 (2017).
60. Padisák, J. & Koncsos, L. Trend and noise: long-term changes of phytoplankton in the Keszthely Basin of Lake Balaton, Hungary. *Int. Assoc. Theor. Appl. Limnol.* **28**, 194–203 (2002).
61. Tátrai, I., Istvánovics, V., Tóth, L.-G. & Kóbor, I. Management measures and long-term water quality changes in Lake Balaton (Hungary). *Fundam. Appl. Limnol.* **172**, 1–11 (2008).
62. Mioni, C., Kudela, R., Baxa, D. & Sullivan, M. *Harmful Cyanobacteria Blooms and their Toxins in Clear Lake and the Sacramento-San Joaquin Delta (California)* (Central Valley Regional Water Quality Control Board, 2011).
63. Winder, M., Reuter, J. & Schladow, G. *Clear Lake Historical Data Analysis* (Univ. California, Davis, 2010).
64. North, R. L. et al. The state of Lake Simcoe (Ontario, Canada): the effects of multiple stressors on phosphorus and oxygen dynamics. *Inland Waters* **3**, 51–74 (2013).
65. Evans, D. O., Skinner, A. J., Allen, R. & McMurtry, M. J. Invasion of zebra mussel, *Dreissena polymorpha*, in Lake Simcoe. *J. Great Lakes Res.* **37**, 36–45 (2011).
66. Baranowska, K. A., North, R. L., Winter, J. G. & Dillon, P. J. Long-term seasonal effects of dreissenid mussels on phytoplankton in Lake Simcoe, Ontario, Canada. *Inland Waters* **3**, 285–296 (2013).
67. Schindler, D. W., Hecky, R. E. & McCullough, G. K. The rapid eutrophication of Lake Winnipeg: greening under global change. *J. Great Lakes Res.* **38**, 6–13 (2012).
68. Allinger, L. & Reavie, E. The ecological history of Lake Erie as recorded by the phytoplankton community. *J. Great Lakes Res.* **39**, 365–382 (2013).
69. Nilson, E. *Investigating Potential Agricultural-related Causes of Eutrophication in the Tsimlyansk Reservoir through GIS and Remote Sensing*. MSc thesis, Central European Univ. (2014).
70. Pozzer, A. et al. AOD trends during 2001–2010 from observations and model simulations. *Atmos. Chem. Phys.* **15**, 5521–5535 (2015).
71. Guan, X., Li, J. & Booty, W. G. Monitoring Lake Simcoe water clarity using Landsat-5 TM images. *Water Resour. Manage.* **25**, 2015–2033 (2011).
72. Belovsky, G. E. et al. The Great Salt Lake Ecosystem (Utah, USA): long term data and a structural equation approach. *Ecosphere* **2**, art33 (2011).
73. Havens, K. et al. Extreme weather events and climate variability provide a lens to how shallow lakes may respond to climate change. *Water* **8**, 229 (2016).
74. Chin, M. et al. Multi-decadal aerosol variations from 1980 to 2009: a perspective from observations and a global model. *Atmos. Chem. Phys.* **14**, 3657–3690 (2014).
75. Ginoux, P., Prospero, J. M., Gill, T. E., Hsu, N. C. & Zhao, M. Global-scale attribution of anthropogenic and natural dust sources and their emission rates based on MODIS deep blue aerosol products. *Rev. Geophys.* **50**, RG3005 (2012).
76. Wang, J., Dai, A. & Mears, C. Global water vapor trend from 1988 to 2011 and its diurnal asymmetry based on GPS, radiosonde, and microwave satellite measurements. *J. Clim.* **29**, 5205–5222 (2016).
77. Tiffany, M. A., Ustin, S. L. & Hurlbert, S. H. Sulfide eruptions and gypsum blooms in the Salton Sea as detected by satellite imagery, 1979–2006. *Lake Reserv. Manage.* **23**, 637–652 (2007).
78. Chang, N.-B., Bai, K. & Chen, C.-F. Smart information reconstruction via time-space-spectrum continuum for cloud removal in satellite images. *IEEE J. Sel. Top. Appl. Earth Obs. Remote Sens.* **8**, 1898–1912 (2015).
79. Wei, Y. et al. NACP MsTMIP: Global and North American Driver Data for Multi-Model Intercomparison. <https://doi.org/10.3334/ORNLDAC/1220> (ORNL DAAC, 2014).
80. Center for International Earth Science Information Network - CIESIN - Columbia University. Gridded Population of the World, Version 4 (GPWv4): Population Density. <https://doi.org/10.7927/H4NP22DQ> (NASA Socioeconomic Data and Applications Center (SEDAC), 2016).

**Acknowledgements** We thank T. Ballard and D. Del Giudice for discussions and input, Y. Fang and E. Sinha for help with obtaining and processing environmental driver datasets, as well as N. Gorelick and T. A. Erickson for guidance with Google Earth Engine. This research was supported by the National Science Foundation (NSF) under grant 1313897. Additional support was provided by the Natural Sciences and Engineering Research Council of Canada (NSERC) under a Postgraduate Scholarship-Doctoral award (PGSD3-438855-2013), by a 2015 Google Earth Engine Research Award, by NASA ROSES grant NNX16AI16G and by USGS Landsat Science Team Award 140G0118C001. CRU-NCEP precipitation was provided by the Multi-scale synthesis and Terrestrial Model Intercomparison Project (MsTMIP: <http://nacp.ornl.gov/MsTMIP.shtml>). Funding for the MsTMIP activity was provided through NASA grant NNX10AG01A. Data management support for preparing, documenting and distributing model driver data was performed by the Modeling and Synthesis Thematic Data Center at Oak Ridge National Laboratory (ORNL; <http://nacp.ornl.gov>), with funding from NASA grant NNH10AN681.

**Author contributions** J.C.H. and A.M.M. designed the research and analysed the results. J.C.H. and A.M.M. wrote the manuscript with input from N.P. J.C.H. performed the majority of the computations with input from A.M.M. N.P. performed the MODTRAN simulations, analysed the MODTRAN results and wrote the corresponding sections of the Methods.

**Competing interests** The authors declare no competing interests.

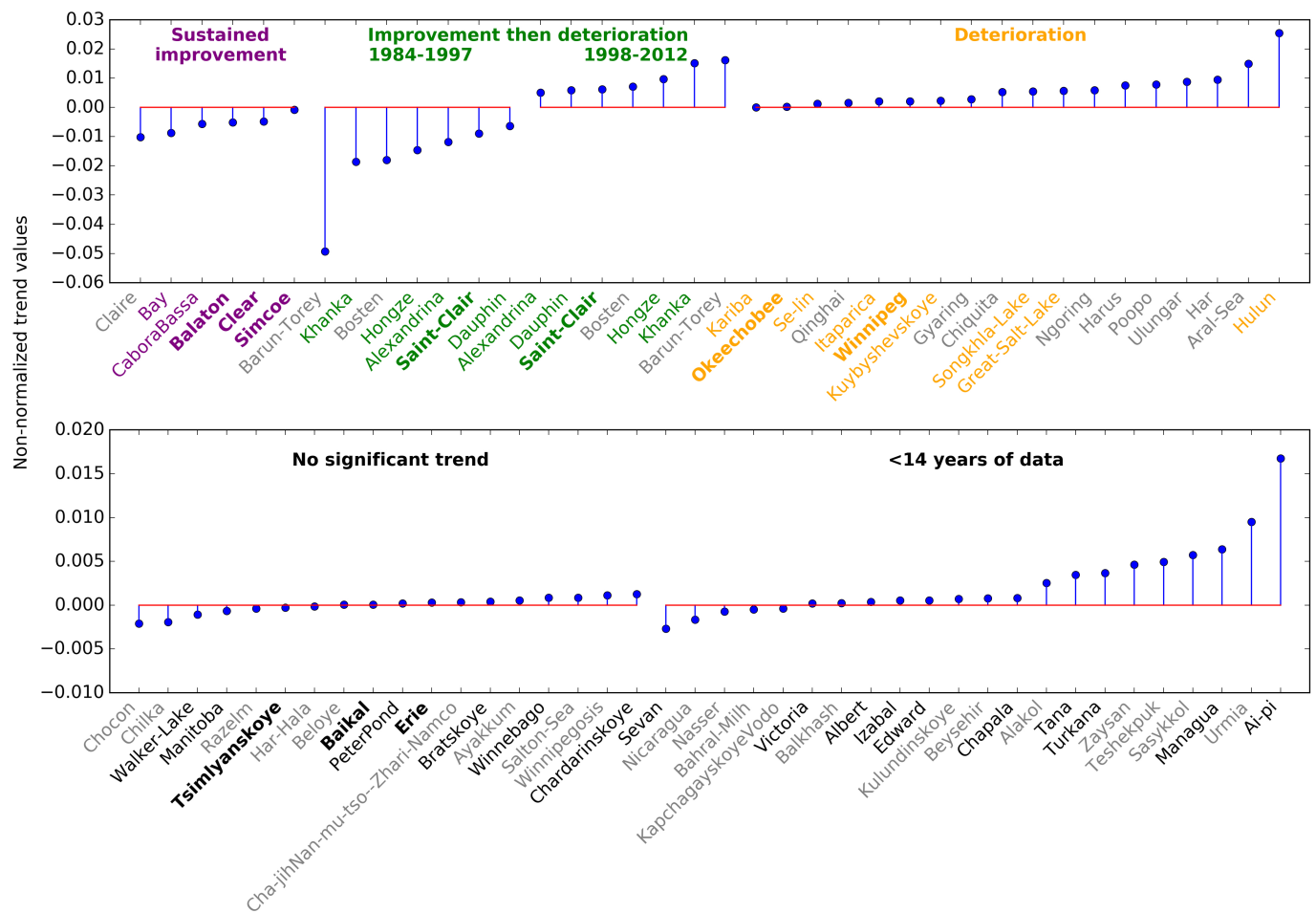
### Additional information

**Supplementary information** is available for this paper at <https://doi.org/10.1038/s41586-019-1648-7>.

**Correspondence and requests for materials** should be addressed to J.C.H. or A.M.M.

**Peer review information** *Nature* thanks Xi Chen and the other, anonymous, reviewer(s) for their contribution to the peer review of this work.

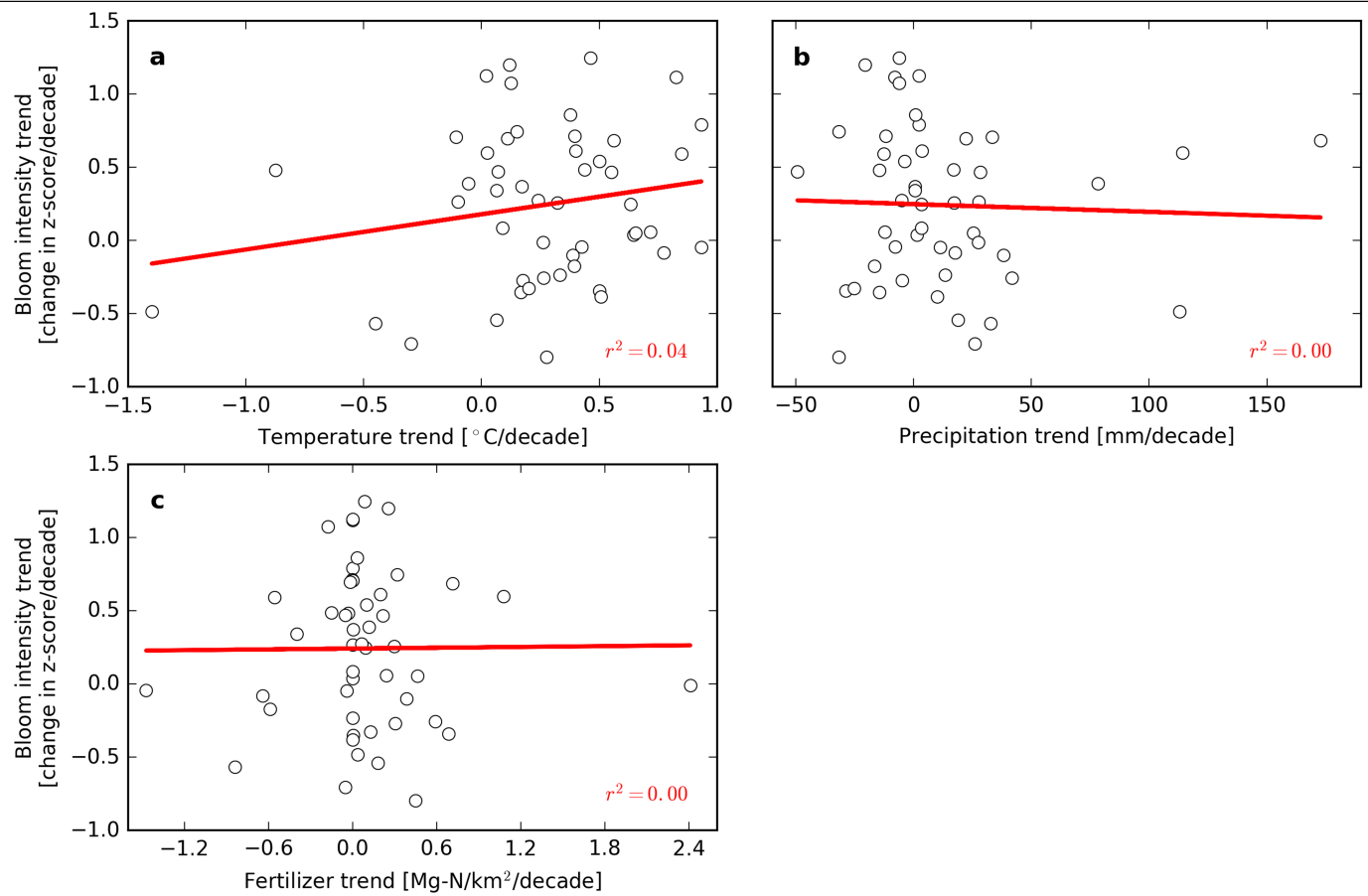
**Reprints and permissions information** is available at <http://www.nature.com/reprints>.



**Extended Data Fig. 1 | Lakes with evidence of cyanobacteria and with well documented evidence of major ecological changes show trends of a similar magnitude to the trends in other lakes.** Lake names in colour indicate that there is evidence of cyanobacteria in that lake; bold lake names indicate that there is evidence of major ecological changes. The y axis shows temporal trends in peak bloom intensity before normalization for all 71 study lakes, categorized

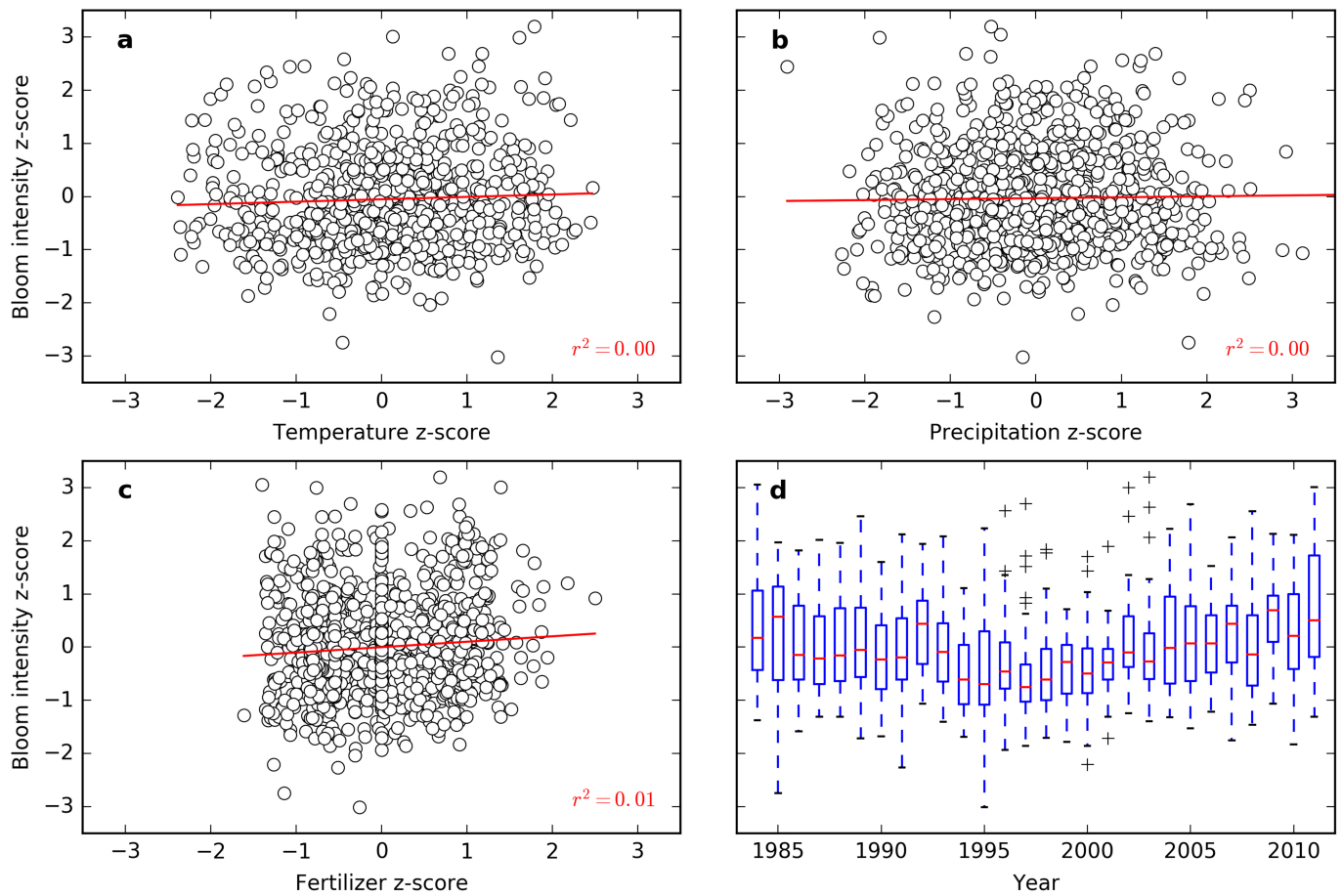
by historical pathway. These temporal trends are the Thiel–Sen's slope values calculated using the maximum summertime lake-wide bloom intensity time series for each lake. Trends for lakes of the ‘improvement then deterioration’ pathway are separated into trends for 1984–1997 and 1998–2012 to show trend values in each sub-period separately.

# Article



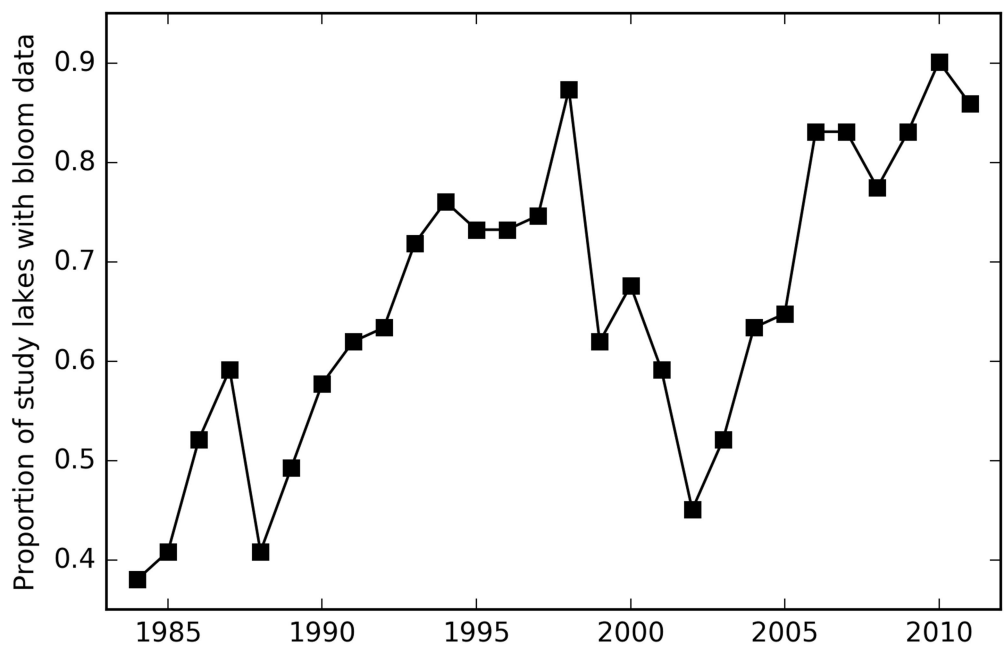
**Extended Data Fig. 2 | Low correlations between trends in bloom intensity and environmental factors.** a–c, Scatter plots of the trend in bloom intensity compared with the trends in temperature (a), total precipitation (b) and

fertilizer application (c) for study lakes with at least 14 years of data ( $n=49$ ). Each circle represents one lake. Red lines indicate the linear fit of the white circles.

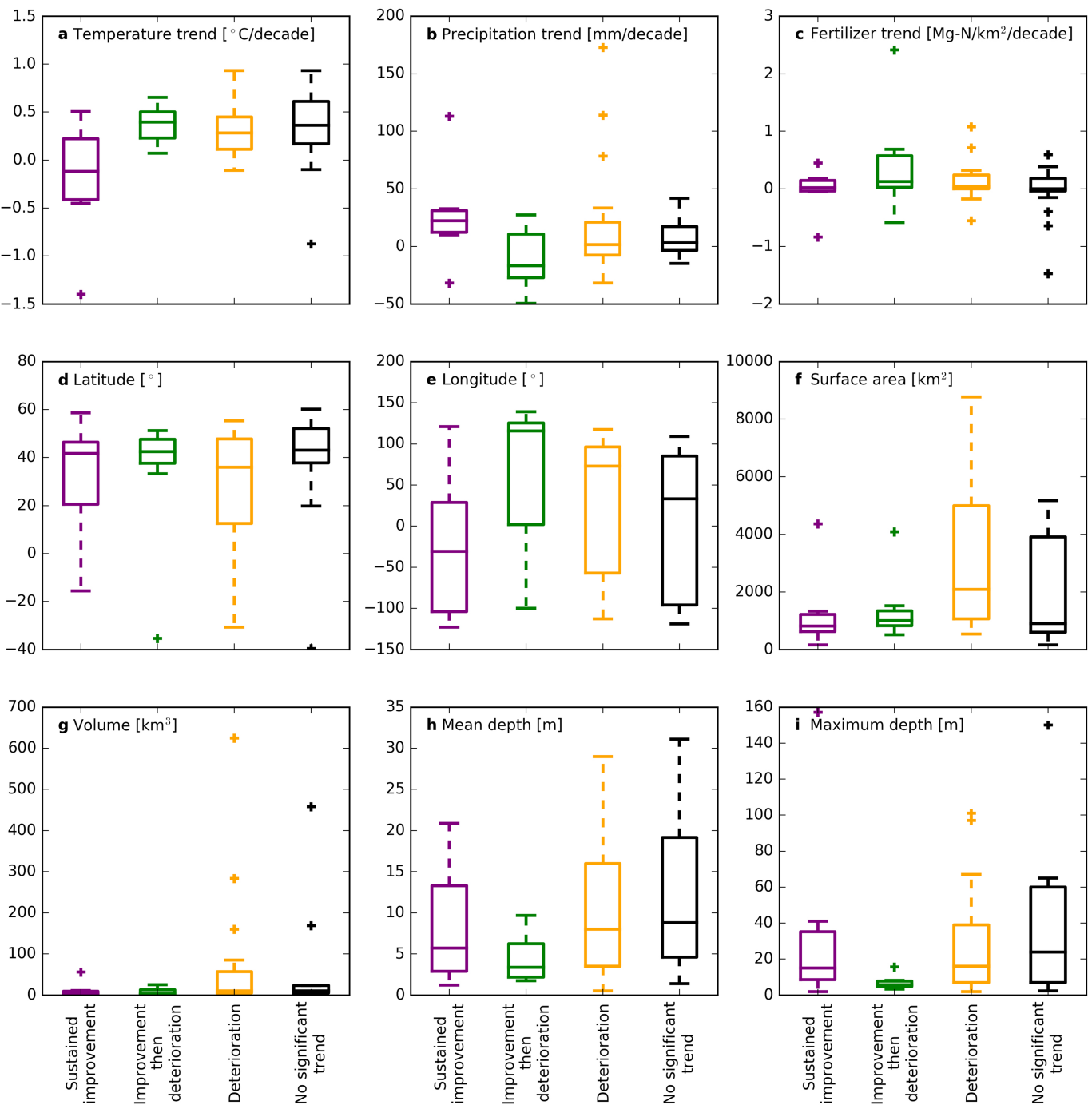


**Extended Data Fig. 3 | No relationship is observed between bloom intensity and environmental factors collected from all lakes.** **a–c,** Scatter plots of bloom intensity z-score compared with temperature (**a**;  $n=784$ ), precipitation (**b**;  $n=936$ ) and fertilizer (**c**;  $n=980$ ) z-scores. Each circle represents one year for one lake. The z-score of each lake variable is calculated using the mean and s.d. of its own time series. Red lines indicate the linear fit of the white circles. **d,** Box

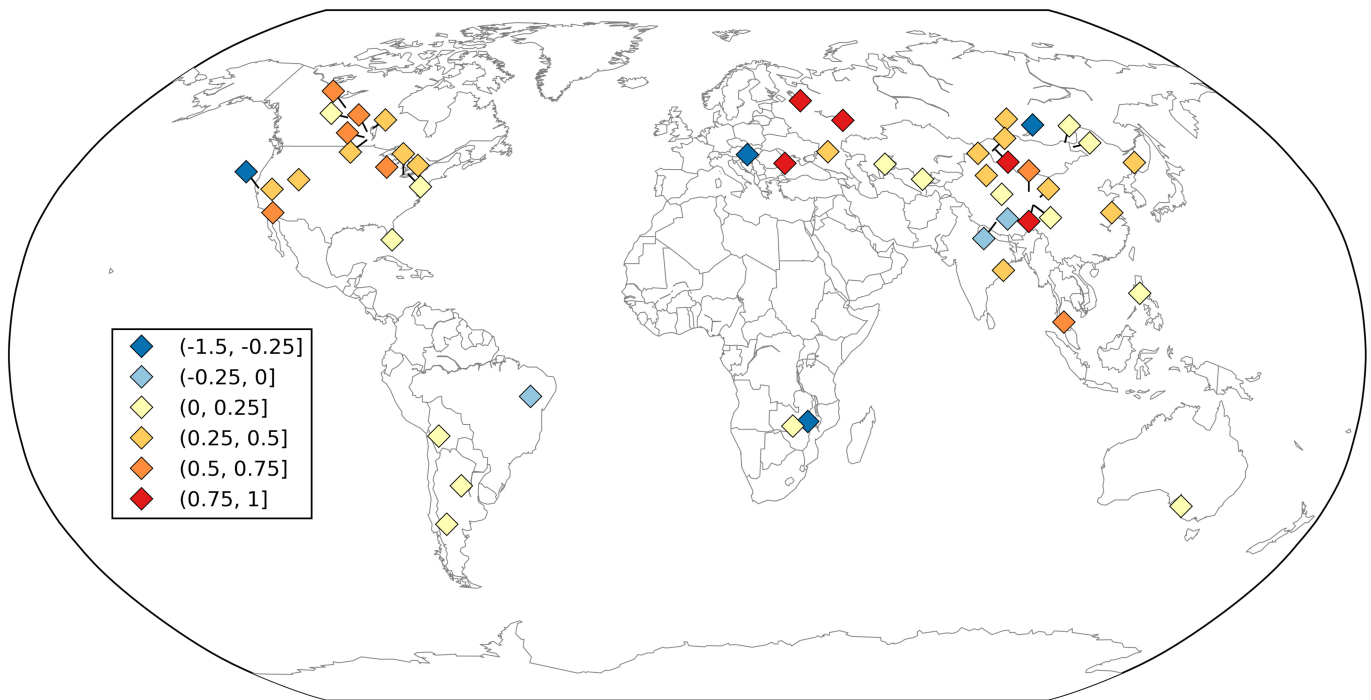
plots of bloom intensity z-score ( $n=980$  total). Each box plot shows the distribution of z-scores for all lakes with available data each year. Each box extends from the first to the third quartile values, with a line at the median. The whiskers extend to  $1.5 \times$  the interquartile range from the edges of the box. The plus symbols show outlier values past the end of the whiskers.



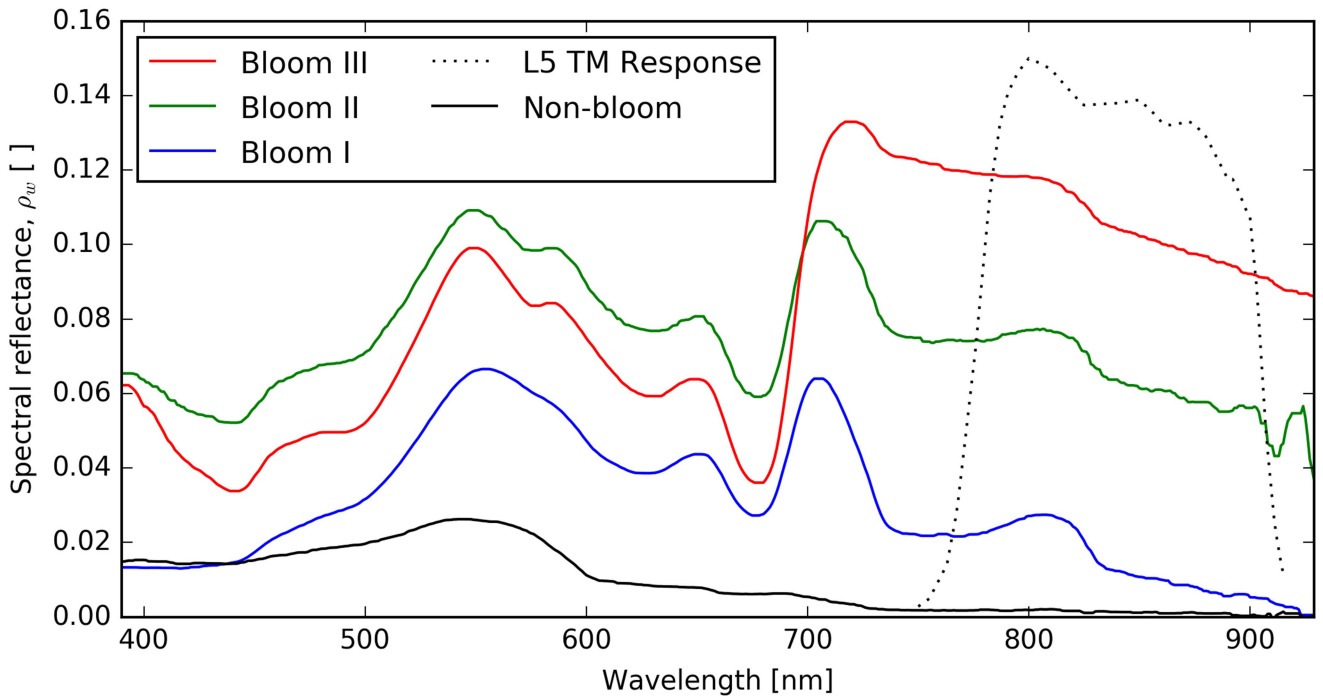
**Extended Data Fig. 4 | Availability of bloom intensity data during the study period.** Number of lakes with a bloom intensity observation after correction for clouds and number of composites (see Methods) divided by the total number of study lakes ( $n=71$ ) for each year.



**Extended Data Fig. 5 | Distributions of lake variables by historical pathway.** **a–c**, Distributions of environmental drivers. **d–i**, Distributions of geomorphological factors. The data in **a** are equivalent to those in Fig. 3.

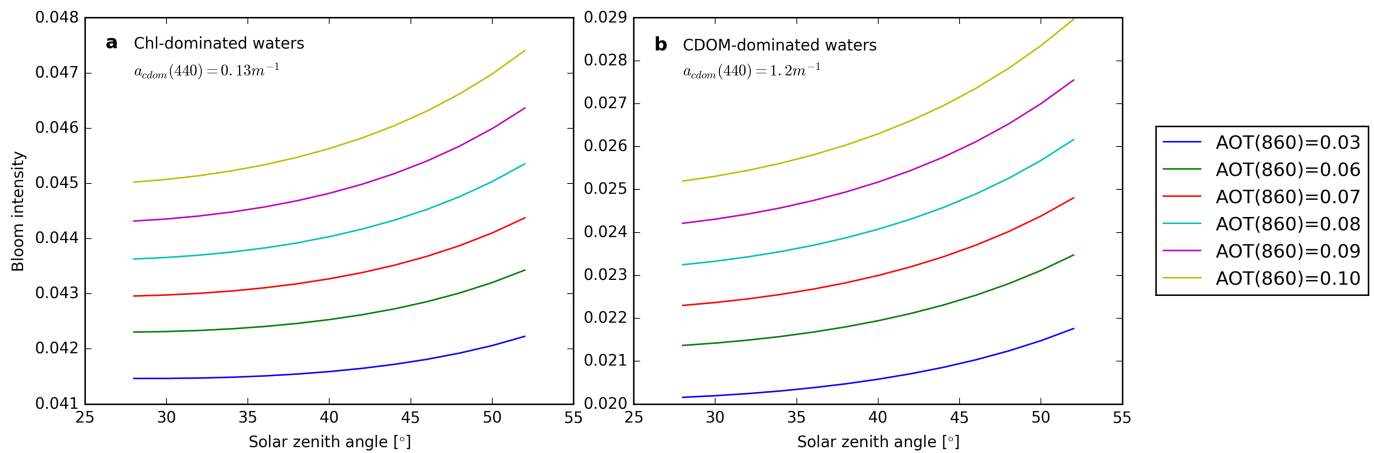


**Extended Data Fig. 6 | Global distribution of trends in lake temperature.** For the lakes with at least 14 years of bloom data ( $n=49$ ), the maps show the temporal trend in lake surface water temperature ( $^{\circ}\text{C}$  per decade). The base map was generated using Generic Mapping Tools<sup>33</sup>.



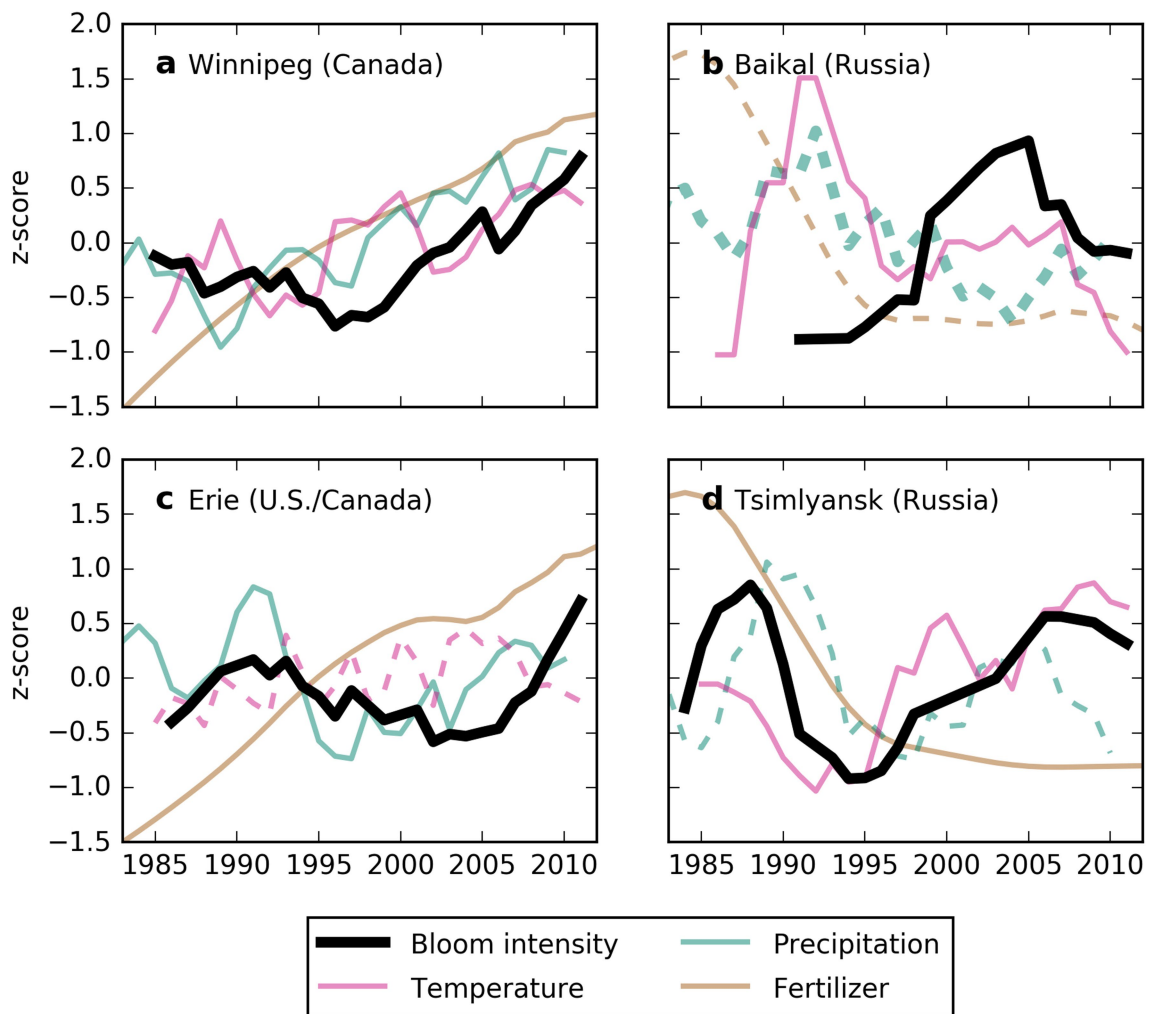
**Extended Data Fig. 7 | Spectral reflectance curves used in simulations to test algorithm sensitivity.** Spectral reflectance curves ( $\rho_w$  [-]) associated with three phytoplankton bloom concentrations and one non-bloom water condition measured in Lake Erie are shown<sup>44</sup>. Blooms I, II and III correspond to near-surface chlorophyll- $a$  concentrations of  $100.1 \text{ mg m}^{-3}$ ,  $143.7 \text{ mg m}^{-3}$  and  $106.3 \text{ mg m}^{-3}$ , respectively, and total suspended solid concentrations of  $30.1 \text{ g m}^{-3}$ ,  $20.0 \text{ g m}^{-3}$

and  $22.7 \text{ g m}^{-3}$ , respectively. The non-bloom curve corresponds to chlorophyll- $a$  and total suspended solid concentrations of  $5.8 \text{ mg m}^{-3}$  and  $1.8 \text{ g m}^{-3}$ , respectively. The normalized spectral response of the near-infrared channel of L5 TM is also shown. The spectra used in the sensitivity analyses demonstrate the robustness of the bloom intensity measure used in this study (Eq. (2)).



**Extended Data Fig. 8 | Observed bloom intensity shows minimal sensitivity to changes in aerosol optical thickness (AOT) or to changes in the solar zenith angle that would result from a change in Landsat 5 orbit.** **a, b,** The sensitivity of derived bloom intensity varies on the order of 0.001 for waters dominated by chlorophyll (Chl) (**a**) and coloured dissolved organic matter

(CDOM) (**b**) for changes in solar zenith angle that would be expected owing to a change in satellite orbit. The simulated variation due to solar zenith angle is even smaller for coarse aerosol types (that is, smaller values of AOT). The environments in **a** and **b** correspond to bloom III and bloom I, respectively, in Extended Data Fig. 7.



**Extended Data Fig. 9 | Historical bloom intensity patterns for four additional lakes with well documented temporal trends.** Graphs as in Fig. 4 for four additional lakes that had well documented temporal trends. Panels show five-year moving averages of normalized bloom intensity, summer lake

temperatures, and total precipitation and fertilizer application rate over each lake's watershed. Thicker temperature, precipitation and fertilizer lines indicate that the Pearson correlation coefficient with bloom intensity is significant ( $P < 0.1$ ). Dashed lines indicate anti-correlations.